Title	Kinematic modeling and error sensitivity analysis for on-machine five-axis laser scanning measurement under machine geometric errors and workpiece setup errors
Author(s)	Ibaraki, Soichi; Goto, Shunsuke; Tsuboi, Keisuke; Saito, Naoto; Kojima, Noriaki
Citation	The International Journal of Advanced Manufacturing Technology , 96 : 4051 - 4062
Issue Date	2018-03-17
DOI	10.1007/s00170-018-1874-4
Self DOI	
URL	https://ir.lib.hiroshima-u.ac.jp/00048864
Right	© Springer-Verlag London Ltd., part of Springer Nature 2018 This is a post-peer-review, pre-copyedit version of an article published in The International Journal of Advanced Manufacturing Technology. The final authenticated version is available online at: https://doi.org/10.1007/s00170-018-1874-4 This is not the published version. Please cite only the published version. この論文は出版社版でありません。引用の際には出版社版をご確認、ご利用ください。
Relation	

Kinematic modelling and error sensitivity analysis for on-machine five-axis laser scanning measurement under machine geometric errors and workpiece setup errors

Soichi Ibaraki

Department of Mechanical Systems Engineering,
Hiroshima University,
Kagamiyama 1-4-1, Higashi Hiroshima, Hiroshima 739-8527, Japan

E-mail: ibaraki@hiroshima-u.ac.jp

Shunsuke Goto

Department of Micro Engineering,
Kyoto University,
Katsura, Nishigyo-ku, Kyoto 615-8530, Japan

Keisuke Tsuboi, Naoto Saito, Noriaki Kojima

Komatsu Ltd.
3-1-1 Ueno, Hirakata-shi, Osaka 573-1011, Japan.

Abstract. On-machine scanning measurement of workpiece geometry has a strong advantage in its efficiency, compared to conventional discrete measurement using a touch-trigger probe. When a workpiece is rotated and tilted, position and orientation errors of the workpiece with respect to the machine's rotary axes can be a significant contributor to the measurement error. Rotary axis geometric errors also influence the measurement error. To establish the traceability of on-machine measurement with workpiece rotation, this paper kinematically formulates their contribution to measured profiles. As a practical application example, this paper presents the measurement error assessment for an axis-symmetric part. Based on the present kinematic model, this paper compares error contributors to the cases 1) where an axis-symmetric part is placed concentric to the rotary axis, and 2) where it is placed away from the rotary axis.

Keywords:
On-machine measurement; laser displacement sensor; geometric errors; kinematic model; five-axis machine tools

1. Introduction

On-machine measurement of workpiece on a machine tool can be employed at different stages of the manufacturing cycle, e. g. 1) post-machining measurement of the machined workpiece for machining accuracy validation, and 2) pre-machining or in-process measurement of workpiece setup or geometry to optimize an NC program. Although a touch-trigger probe is still more common in today's manufacturing industry, continuous profile measurement using a non-contact optical displacement sensor has gained more attention in various manufacturing applications. A good review has been published by Savio et al. [1] and Schwenke et al. [2]. Shacham et al. [3] and Nishikawa et al. [4] presented its application in aircraft parts manufacturing. On five-axis machine tools, when the orientation of the workpiece or the sensor is regulated by rotary axes as shown in Fig. 1, the entire 3D geometry can be measured with the laser beam regulated perpendicular to the target surface. Lately, particularly for large-sized parts, a machine tool can be employed as a comparator to measure its geometry during the manufacturing process [5, 6]. Such a new industrial application shows a potential applicability of a machine tool as a coordinate measuring machine (CMM) [7, 8]. A good review on existing on-machine measurement technologies has been published by Mutilba et al. [8] and Takaya [9].

A critical issue with the measurement process on a machine tool is the lack of the traceability. Recently, research efforts have been reported to establish the traceability chain for on-machine measurement. Schmitt et al. [10] presented the combination of the traceability establishment for a CMM and innovative calibration methods for machine tools. Acko et al. [11] and Viprey et al. [12] presented an artefact to establish the traceability for on-machine probing. A review can be found in [8]. In principle, the traceability of on-machine measurement can be ensured by assessing its measurement uncertainty in the same way as for CMMs; the methods for the measurement uncertainty assessment for CMMs are described in ISO 15530-3 [13] and 15530-4 [14]. Compared to CMMs, a big challenge for a traceable machine tool measurement is non-controlled shop floor environment [8]. In particular, thermal effects can be a dominant uncertainty source.

In three-axis measurement using linear axes only, setup errors of workpiece, i.e. position and orientation errors of a workpiece on a work table, are not a critical issue. They simply translate or tilt the measured profile. On the other hand, in five-axis measurement, they change the position and the orientation of workpiece with respect to rotary axis average lines, and thus can give a significant impact to the measured geometry. When a workpiece is machined and then measured on the same machine, workpiece setup errors may not influence the measurement uncertainty at all. In industrial applications, a workpiece is often machined by multiple machine tools, e.g. a machining center and a grinding machine. In such a case, workpiece setup errors on the measuring machine can be a critical uncertainty contributor. Furthermore, in three-axis measurement, error motions of linear axes are basically copied as the geometric error

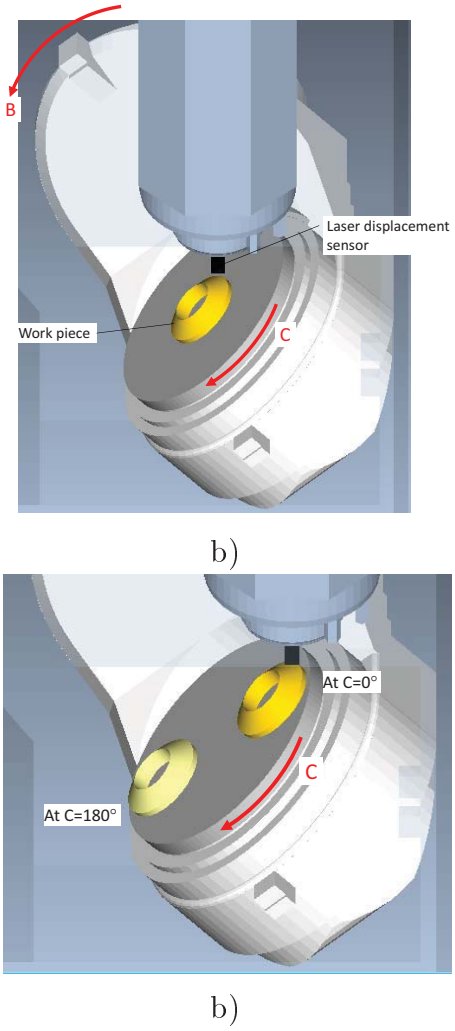

Figure 1. Typical setups of on-machine profile measurement for an axis-symmetric workpiece. a) When an axis-symmetric part placed concentric to the C-axis of rotation, a single circular profile can be measured with rotating C-axis only. b) When it is placed away from the axis of rotation, linear axes (X, Y, Z) must be driven synchronously.

in measured profiles. When rotary axes are involved, this relationship becomes more complex. To understand this relationship, the five-axis kinematic model is essential.

As a basis to establish a traceability chain for measurement on a five-axis machine tool with workpiece rotation, this paper presents a kinematic model to describe contributions of machine geometric errors and workpiece setup errors to the error of measured profiles. As a practical application example, this paper studies the measurement uncertainty assessment for an axis-symmetric part. As shown in Fig. 1, the swivel axis (B-axis) is regulated such that the laser displacement sensor's sensitive direction becomes normal to the workpiece surface. When an axis-symmetric part is placed concentric to the rotary axis, its profile can be measured with continuously rotating one rotary axis only (see Fig. 1a), and thus the contribution of the machine's error motions on the measurement uncertainty can be minimized. However, the

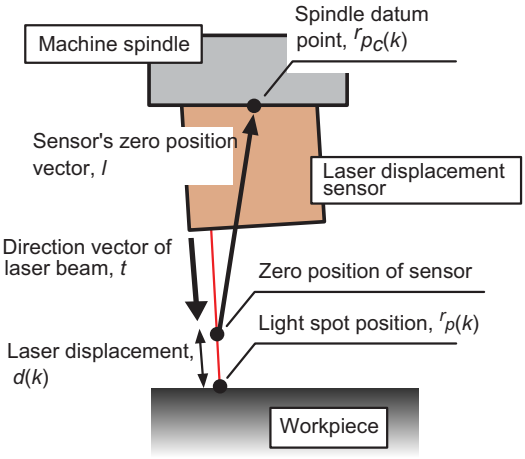

Figure 2. Optical sensor setup to measure the light spot position, $^{r}p(k)$ [19].

workpiece's setup errors can impose significant influence on the measurement error. On the other hand, when the workpiece is placed away from the axis of rotation, linear axes (X, Y, Z) must be driven synchronously (see Fig. 1b). Then, many contributors impose more influence. The paper demonstrates the application of the present kinematic model to evaluate such contributions.

The kinematic model of five-axis configurations has been studied since the 1980s and used in many previous literature as a basis for machine tool metrology, e.g. Hocken et al. [15], Reshetov et al. [16], Abbaszaheh-Mir et al. [17], Inasaki et al. [18]. A part of the authors presented the kinematic formulation of five-axis measurement in [19, 20]. This paper's original contributions are as follows: 1) the five-axis measurement is modelled with both the machine's geometric errors and the workpiece's setup errors in a unified manner. 2) Its application to the sensitivity analysis of potential error causes to scanning measurement of an axis-symmetric part is presented. As a case study, on-axis and off-axis scanning measurements are compared from the viewpoint of the contribution of the machine's geometric errors and the workpiece's setup errors. 3) Its practical application is experimentally demonstrated.

2. On-machine five-axis measurement setup

Figure 2 depicts a typical setup of optical profile measurement system considered in this paper [19, 20]. The light spot position, i.e. the intersection of the laser beam axis and the object surface, is denoted by $^{r}p(k) \in \mathbb{R}^3$ and given as follows:

$$^{r}p(k) = {}^{r}p_c(k) - \hat{l} - d(k) \cdot \hat{t} \tag{1}$$

where *the direction vector of the laser beam*, $\hat{t} \in \mathbb{R}^3$, is a unit vector representing the sensor's sensitive direction. $\hat{l} \in \mathbb{R}^3$ represents a vector from the sensor's zero point to the spindle datum point, and is hereafter called *the sensor's zero position vector*. $^{r}p_c(k) \in \mathbb{R}^3$ represents the position of the intersection of the spindle axis average line [21] and the

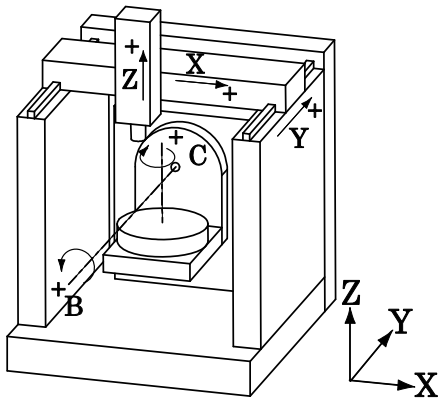

Figure 3. Machine configuration [19].

spindle gauge line, called *the spindle datum point* hereafter. Linear encoder X, Y, and Z positions are logged in the CNC system, synchronously with the laser displacement, $d(k)$, at the k-th sampling point. This (X, Y, Z) position represents ${}^{r}p_c(k)$ in the Machine Coordinate System (MCS). Throughout this paper, the left-hand side superscript ^{r} denotes a vector represented in the MCS. This paper considers a five-axis machine with two rotary axes in the workpiece side (see Fig. 3). The *Workpiece Coordinate System* (WCS) is a local coordinate system attached to the rotary table, with its origin at the nominal intersection of B- and C-axis centerlines. The left-hand side superscript ^{w} denotes a vector represented in the WCS.

Laser displacement sensors typically exhibit the best measurement performance when the measured surface is placed normal to the sensor's sensitive direction. The B- and C-axes are commanded to the angular positions, $B(k)$ and $C(k) \in \mathbb{R}$ such that the workpiece surface's normal vector at the light spot position becomes nominally parallel to the laser beam direction vector, $\hat{t}$. Suppose that the k-th point on the workpiece's nominal surface is given by ${}^{w}p^*(k) \in \mathbb{R}^3$ in the workpiece coordinate system. In this paper, the workpiece's "nominal" surface represents the assumed surface based on which the measuring command trajectory, ${}^{w}p^*(k)$, is calculated. The upperscript * represents the nominal point calculated from it. When there exists no geometric error of rotary axes, this point is converted to the MCS by:

$$\begin{bmatrix} {}^{r}p^*(k) \\ 1 \end{bmatrix} = {}^{r}T^*_w(B(k), C(k)) \cdot \begin{bmatrix} {}^{w}p^*(k) \\ 1 \end{bmatrix} \tag{2}$$

where ${}^{r}T^*_w(B(k), C(k)) \in \mathbb{R}^{4\times4}$ is the Homogeneous Transformation Matrix (HTM) given by:

$${}^{r}T^*_w(B(k), C(k)) = D_b(-B(k))D_c(-C(k)) \tag{3}$$

where $D_b(B)$ and $D_c(C) \in \mathbb{R}^{4\times4}$ represent the HTM of the rotation, respectively about Y and Z axes. See e.g. [17, 18] for their formulation.

The machine should be commanded such that the spindle datum point, ${}^{r}p^*_c(k)$,

moves along the following trajectory in the MCS:

$$ {}^{r}p_c^*(k) = {}^{r}p^*(k) + \hat{l} \tag{4} $$

3. Kinematic modelling of five-axis profile measurement under machine geometric errors and workpiece setup errors

3.1. Objective

The objective is to build a model to describe the laser displacement, $d(k)$ in Eq. (1), when there exist the following errors:

(1) *Machine geometric errors:*

For the simplicity of the formulation, this paper only considers position and orientation errors of rotary axis average lines shown in Table 1 (called *location errors* in ISO 230-7 [21]). The axis average line of a rotary axis represents the mean position and orientation of the axis of rotation over full rotation [22]. For example, in Table 1, the orientation error of the B-axis average line with respect to the machine coordinate system, or equivalently, the squareness error of the B-axis average line to the Z-axis reference line, is represented by the notation α^0_{BR}, or E_{A0B} according to the notation in ISO 230-1 [22]. ISO 230-1 [22] describes in details the definition of all the geometric errors in Table 1.

The model to be presented in this paper can be straightforwardly extended to more general position-dependent geometric errors (analogous extension of the kinematic model was presented in [23]).

(2) *Workpiece setup errors:*

When there exists no position/orientation error in the workpiece's setup, the workpiece's nominal surface is given by the following function $\Gamma^* \in \mathbb{R}^3 \to \mathbb{R}$ in the WCS:

$$ \Gamma^* \left({}^{w}q^*\right) = 0 \tag{5} $$

where ${}^{w}q^* \in \mathbb{R}^3$ represents a point on the workpiece's surface. With position/orientation errors in the workpiece's setup, its actual surface is represented by:

$$ \Gamma\left({}^{w}q\right) = 0 \tag{6} $$

3.2. Step 1: Position of laser beam in WCS under machine geometric errors

The five-axis kinematic model has been presented in many previous publications, e.g. [16, 17, 18] and thus is reviewed here only briefly. Suppose that the command light spot position is given by ${}^{r}p^*(k)$ in the MCS. Under location errors in Table 1, it is in the WCS at:

$$ \begin{bmatrix} {}^{w}p(k) \\ 1 \end{bmatrix} = \left({}^{r}T_w(B(k), C(k))\right)^{-1} \cdot \begin{bmatrix} {}^{r}p^*(k) \\ 1 \end{bmatrix} \tag{7} $$

Table 1. Position and orientation errors (location errors) of rotary axis average lines for the machine configuration in Fig. 3.

Symbol [18]	Symbol [22]	Description
Location errors associated with rotary axes		
α^0_{BR}	E_{A0B}	Squareness error of B- to Z-axis
β^0_{BR}	E_{B0B}	Angular positioning error of B-axis at $B = 0°$
γ^0_{BR}	E_{C0B}	Squareness error of B- to X-axis
α^0_{CB}	$E_{A0C} - E_{A0B}$	Squareness error of C- to B-axis
δx^0_{BR}	E_{X0B}	Position error of B-axis average line in X direction
δy^0_{BR}	E_{Y0C}	Position error of C-axis average line in Y direction
δz^0_{BR}	E_{Z0B}	Position error of B-axis average line in Z direction
δx^0_{CB}	$E_{X0C} - E_{X0B}$	Linear offset of C-axis from B-axis in X
Location errors associated with linear axes		
γ^0_{YX}	$E_{C(0X)Y}$	Squareness error of Y- to X-axis
α^0_{ZY}	$E_{A(0Y)Z}$	Squareness error of Z- to Y-axis
β^0_{ZX}	$E_{B(0X)Z}$	Squareness error of Z- to X-axis

where ${}^rT_w(B(k), C(k)) \in \mathbb{R}^{4\times4}$ is the HTM from the WCS to the MCS and is given by:

$$\begin{aligned} {}^rT_w(B(k), C(k)) &= {}^rT_b(B(k)){}^bT_c(C(k)) \\ {}^bT_c(C(k)) &= D_x(\delta x^0_{CB})D_a(\alpha^0_{CB})D_c(-C(k)) \\ {}^rT_b(B(k)) &= D_x(\delta x^0_{BR})D_y(\delta y^0_{BR})D_z(\delta z^0_{BR})D_a(\alpha^0_{BR})D_b(\beta^0_{BR})D_c(\gamma^0_{BR})D_b(-B(k)) \end{aligned} \tag{8}$$

3.3. Step 2: Laser displacement under workpiece setup errors in WCS

Due to location errors in Table 1, the nominal laser spot position is displaced from ${}^wp(k)^*$ to ${}^wp(k)$ in Eq. (7). When the workpiece surface is given by a function Γ in Eq. (6), the intersection of the laser beam with the workpiece surface, ${}^w\hat{p}(k) \in \mathbb{R}^3$, can be calculated by solving:

$$\begin{aligned} &\Gamma\left({}^w\hat{p}(k)\right) = 0 \\ &\text{where} {}^w\hat{p}(k) = {}^wp(k) + \hat{d}(k) \cdot {}^w\hat{l} \end{aligned} \tag{9}$$

This gives the influence of location errors in Table 1 on the laser displacement, $\hat{d}(k) \in \mathbb{R}$. In Eq. (9), ${}^w\hat{l} \in \mathbb{R}^3$ represents a unit vector representing the laser beam direction in the WCS. Typically it is set to the normal direction of the workpiece surface at ${}^wp^*(k)$. Rotary axis location errors affect ${}^w\hat{l}$, since it is defined with respect to the workpiece coordinate system, but its influence is usually negligibly small.

4. A case study

4.1. Workpiece and on-machine measurement setup

As a practical application example, this paper demonstrates on-machine geometric measurement of a part shown in Fig. 4. The conical surfaces A and B are measured.

The nominal conical angle is 0.01 mm/2 mm$\approx 0.28^\circ$ for the surface A and 3.6° for the surface B with respect to the datum bottom surface C. In both setups, three concentric circular lines on Surface A of the radius $r_c(1) = 71.0$, $r_c(2) = 70.5$, $r_c(3) = 70.0$ mm, and three lines on Surface B of the radius $r_c(4) = 68.5$, $r_c(5) = 66.5$, $r_c(6) = 64.5$ mm, were measured. See Fig. 7a for the six measured circular lines.

In industrial manufacturing lines of this workpiece, it is first semi-finished on a turning center or a machining center, and then finished on a grinding center. Finally, it is loaded on a five-axis machine for geometric inspection. The workpiece setup error may be introduced with the loading of the workpiece. It can be a significant error contributor to machining and grinding processes, and also the measurement process. Furthermore, a single workpiece is load on the measuring machine, it can be placed concentric to the rotary table's axis (C-axis.) When multiple workpieces are loaded for higher efficiency, it must be placed away from the C-axis. This case study considers both setups:

Setup (1): *Measurement with C-axis rotation only, with the workpiece placed concentric to a rotary table's axis of rotation.*

The workpiece was fixed concentric to a rotary table's axis of rotation (see Fig. 5a). The workpiece's position was adjusted by rotating the workpiece with a dial gauge touching the workpiece's datum cylindrical surface. The uncertainty ($k = 2$) in this adjustment was assessed ± 10 μm (uniform distribution). The C-axis angular velocity was 5108.4°/min. Since the sampling time in the experiment was 1 msec, each sampling point corresponds to about 0.1 mm on circular paths. The B-axis is tilted at $B = 0.28^\circ$ for the surface A and $B = -3.6^\circ$ for the surface B such that the laser beam is nominally perpendicular to the workpiece surface. The command light spot position, ${}^r p$, is at $Y = 0$. In the MCS, none of X-, Y-, and Z-axes moves during each rotation (only C-axis rotates). The spindle rotation is mechanically fixed throughout the experiment.

Setup (2): *Measurement with X, Y, Z and C-axis movement, with the workpiece placed away from C-axis centerline.*

The same workpiece was fixed near the edge of the rotary table (see Fig. 5b). The workpiece's center position was measured as ${}^r q_{center} = (75.453, -77.898)$ mm when $B = 0^\circ$. This measurement was very rough, possibly with the uncertainty ($k = 2$) as large as ± 0.3 mm. The same six concentric circular lines were measured. In the WCS, the nominal trajectory of light spot, ${}^w p^*(k)$, is given by:

$$ {}^w p^*(k) = \begin{bmatrix} r_c(n)\cos(\theta(k)) + {}^r q_{center}(1) \\ r_c(n)\sin(\theta(k)) + {}^r q_{center}(2) \\ z_c(n) \end{bmatrix} \tag{10} $$

where $n \in (1, \cdots 6)$ is the path index number. $z_c(n) \in \mathbb{R}$ is the nominal z-height of the n-th path in the workpiece coordinate system. The B- angular positions are given such that the laser beam is nominally perpendicular to the workpiece surface, namely $B = 0.28^\circ$ for the surface A and $B = -3.6^\circ$ for the surface B. Then, the command trajectory of the spindle datum point in the MCS, ${}^r p_c^*(k)$, is given by Eq. (4). Figure 6

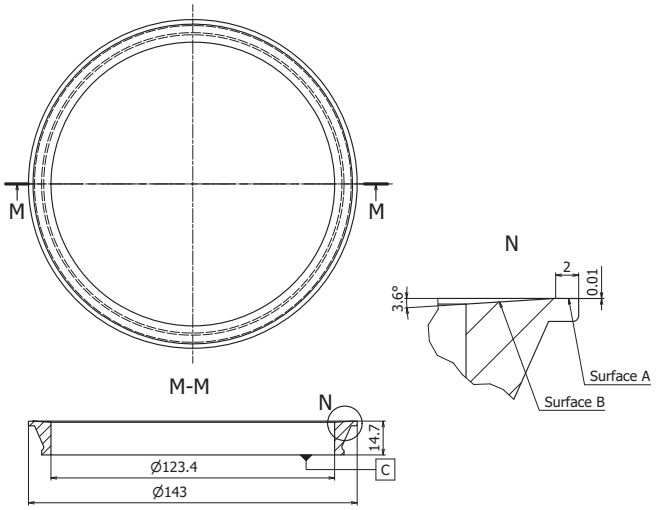

Figure 4. Nominal geometry of workpiece. Only major and relevant dimensions are shown.

shows command X, Y, Z, B and C profiles in the MCS (three concentric paths for the surface A, $n = 1, 2, 3$). It shows that this test requires simultaneous 4-axis motion. The feed speed for each axis is calculated such that the velocity of the light spot in the WCS is 5108.4°/min.

The thermal change in the machine structure or environment often influences error motions of linear axes [24]. It is thus more difficult to ensure the traceability in the on-machine measurement when linear axes are involved, as in Setup (2). Such a setup may be inevitable when, for example, multiple workpieces are fixed on the machine table.

4.2. Measured profiles

Figure 7 shows measured profiles for Setup (1). The measured light spot position in the MCS, ${}^{r}p(k)$, is calculated by Eq. (1) from the measured laser displacement, $d(k)$ and the spindle datum position, ${}^{r}p_c(k)$. Then, it is converted to the WCS by Eq. (2). In Fig. 7a, the error from the nominal geometry is shown by color. In b), nominal circular trajectories are shown by "zero error line." The error is magnified 1,000 times and shown by a polar plot. All of total six lines on the surfaces A and B are shown. Only 290° was measured due to the interference with clamping fixtures (see Fig. 5a). Similarly, Fig. 8 shows measured profiles for Setup (2). The workpiece orientation is the same in both setups.

Each test, measuring six lines, took about four minutes, and thus thermal influence during each test is negligible. Setup (2) was tested after about 2 hours from Setup (1), and thus thermal influence can be larger. The room temperature was controlled within 1°C but the machine temperature change was not measured.

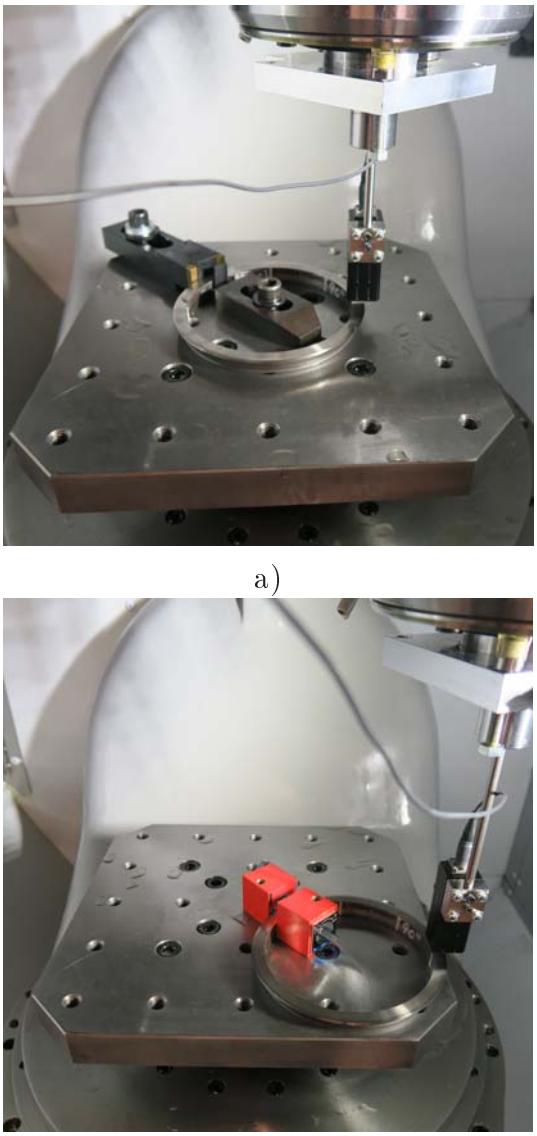

Figure 5. Test setups. a) Setup (1), where the workpiece is placed concentric to C-axis centerline. b) Setup (2), where the workpiece is placed away from C-axis centerline.

Comparison with a circularity measuring machine:

The same workpiece was measured by using a conventional circularity measuring machine. Figure 9 shows the measurement setup. The probe's sensitive direction was tilted from the surface's normal direction by about 30°, and its influence was numerically compensated for. Figure 10 shows measured surface profiles. Table 2 compares the difference between maximum and minimum deviations from the nominal surface profile (see [25] for its definition). On-machine laser measurement in Setup (1) (Fig. 7) showed larger error by about 6 to 8 μm than the circularity measuring machine. This difference may be attributable to the influence of the clamping force in on-machine measurements (the workpiece was not clamped on the circularity measuring machine).

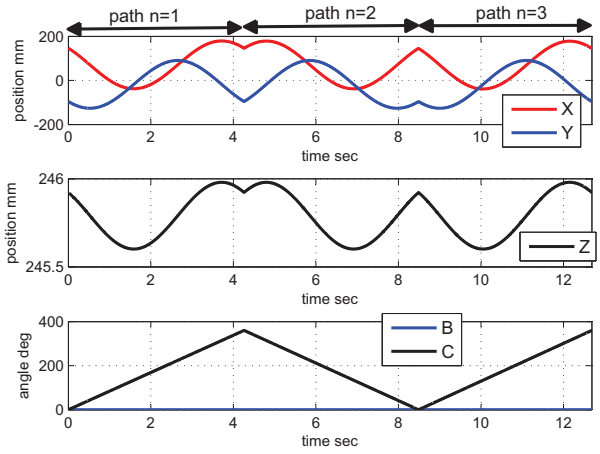

Figure 6. Command X, Y, Z, B and C profiles in the MCS for Setup (2) (three concentric paths for the surface A, $n = 1, 2, 3$).

Figure 12 shows the difference between the measured profiles in Setup (1) (Fig. 7) and (2) (Fig. 8). This difference will be discussed in Section 4.4.

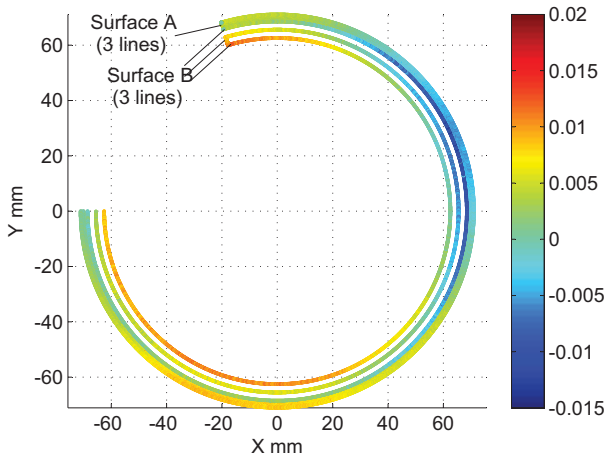

a)

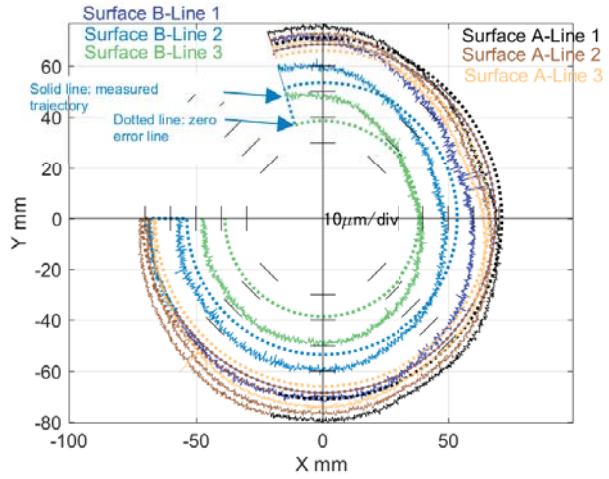

b)

Figure 7. Measured profiles for Setup (1), where the workpiece is placed concentric to C-axis centerline. a) In a color map, b) in a polar plot. In b), the measured profile error is magnified 1,000 times and plotted in the radial direction. "Zero error lines" represent nominal trajectories on the workpiece surface. Their actual pitch is 0.5 mm for the surface A and 2 mm for the surface B, but it is magnified in b) for clarification.

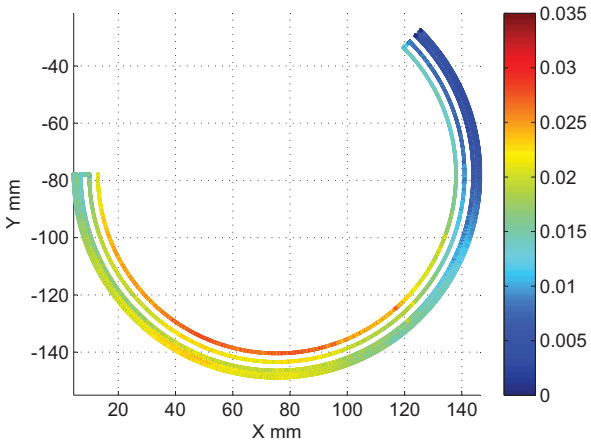

a)

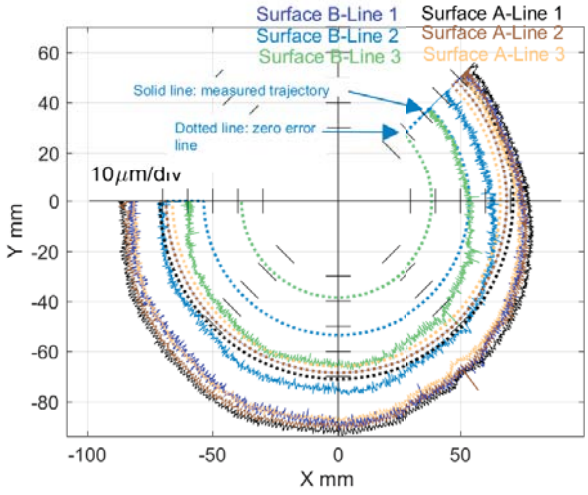

b)

Figure 8. Measured profiles for Setup (2), where the workpiece is placed away from C-axis centerline. a) In a color map, b) in a polar plot.

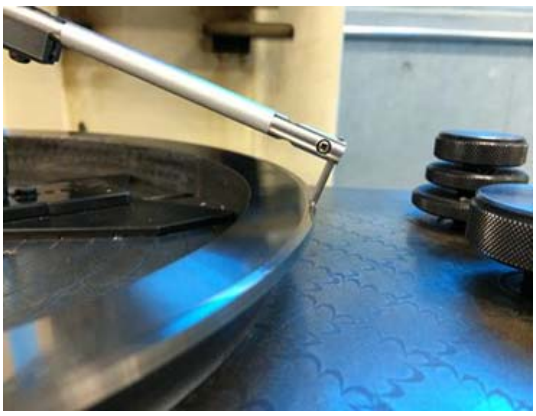

Figure 9. Measurement setup on a circularity measuring machine.

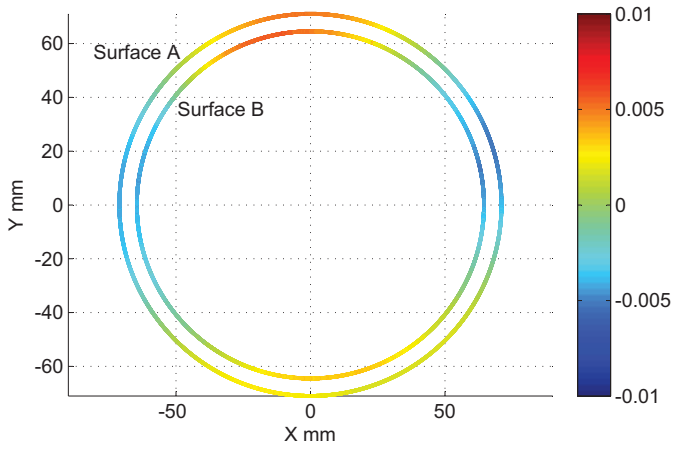

Figure 10. Surface profiles measured by a circularity measuring machine.

Table 2. Comparison in the difference between maximum and minimum deviations from the nominal surface profile.

	Surface A	Surface B
By circularity measuring machine	9.0 μm	9.6 μm
On-machine laser measurement (Setup (1))	15.3 μm	17.1 μm
On-machine laser measurement (Setup (2))	20.9 μm	23.2 μm

4.3. Sensitivity analysis of machine geometric errors and workpiece setup errors

The analysis objective is to calculate the influence of 1) workpiece setup errors, e_x, e_y, e_a, and e_b, and 2) location errors of linear and rotary axis average lines, shown in Table 1, on the measured surface profile, ${}^w\hat{p}(k)$, given in Eq. (9).

These influences can be calculated by the formulation presented in Sections 3.2 and 3.3. Additionally, the workpiece setup errors, e_x, e_y, e_a, and e_b, can be calculated as follows: When the nominal workpiece is displaced by $(e_x, e_y) \in \mathbb{R}^2$ in X- and Y-directions and tilted by $(e_a, e_b) \in \mathbb{R}^2$ around X- and Y-axes, it is given by:

$$\Gamma({}^wx(k), {}^wy(k), {}^wz(k)) = ({}^wz'(k) - z_0) - m_0 \left(\sqrt{({}^wx'(k) - e_x)^2 + ({}^wy'(k) - e_y)^2} - r_0 \right) = 0 \quad (11)$$

where

$$\begin{bmatrix} {}^wx'(k) \\ {}^wy'(k) \\ {}^wz'(k) \\ 1 \end{bmatrix} = D_a(-e_a) D_b(-e_b) \begin{bmatrix} {}^wx(k) \\ {}^wy(k) \\ {}^wz(k) \\ 1 \end{bmatrix} \quad (12)$$

$m_0 \in \mathbb{R}$ is the nominal cone slant angle. In this case study, $m_0 = -0.01/2$ for the surface A and $m_0 = 3.6 \cdot \pi/180$ for the surface B.

Table 3 shows the simulated difference between maximum and minimum deviations from the nominal surface profile when each error is given either 100 μm or $0.1/10^3$. The following observations can be made:

- When the workpiece is placed concentric to the rotary axis (Setup (1)), linear and rotary axis location errors do not influence the measured profile almost at all.
- When the workpiece is placed away from the axis of rotations (Setup (2)), rotary axis location errors impose more influence on the measured profile. Its influence is still not significant (e.g. $\delta x^0_{BR} = 100$ μm gives 12.6 μm).
- In Setup (1), orientation errors in the workpiece setup, e_a and e_b, are major error contributors. Since the slant angle of surface A is smaller ($m_0 = -0.01/2$), the influence of setup position errors, e_x and e_y, on the surface A is negligibly small.

As examples, Fig. 11 shows the simulated profile errors in Setup (2) under a) the C-axis position error in X, $\delta x^0_{BR} = 100$ μm and b) the workpiece position error in X, $e_x = 100$ μm.

Remark: To evaluate the combined uncertainty under all of the contributors shown in Table 3, the Monte Carlo simulation can be applied according to [26].

Remark: As discussed in Section 1, thermal influence can be generally a major uncertainty for on-machine measurements. The present analysis does not explicitly consider this influence. However, the machine's structural deformation due to the thermal influence can be generally parameterized as the change in rotary axis location errors; Gebhardt et al. [27] and Ibaraki et al. [28] showed it by the R-Test, and Ibaraki et al. [29] showed it by the machining test. For example, when the thermal influence displaces the spindle to -Z direction, it changes the Z-position of the B-axis average line, i.e. δz^0_{BR} in Table 1. To assess the measurement uncertainty due to the thermal influence, first the thermal influence on rotary axis location errors must be experimentally investigated, and then its contribution to the measurement uncertainty can be assessed by using Table 3.

4.4. Diagnosis of possible causes for on-machine measurement error in Setup (2) and their compensation

Since the workpiece is the same, the difference in the measured profiles in Setups (1) and (2) is caused only by machine geometric errors and workpiece setup errors. The measured profiles in Setup (1) (Fig. 7), and (2) (Fig. 8) show significant difference; the mean of the difference is 13.7 μm and its standard deviation is 2.4 μm. Figure 12 shows the difference between the measured profiles in Setups (1) and (2).

From a complete set of simulated profiles in Section 4.3 (including ones shown in Fig. 11) , the following setup errors are found as a potential cause for this measurement error: $e_x = 0.2$ mm and $e_y = -0.2$ mm in Setup (2) ((e_x, e_y): the workpiece position error). Figure 13 shows the simulated influence of $(e_x, e_y) = (0.2, -0.2)$ mm on the profiles in Setup (2). Figure 14 shows measured profiles for Setup (2), where the

Table 3. Simulated difference (in μm) between maximum and minimum deviations from the nominal surface profile. "–" represents a negligibly small vaue (< 0.1 μm). The value in bold represents relatively larger influence.

Symbol	Given value	Setup (1)		Setup (2)	
		Surface A	Surface B	Surface A	Surface B
Rotary and linear axis location errors					
α^0_{BR}	$0.1/10^3$	–	–	**21.7**	**21.9**
β^0_{BR}	$0.1/10^3$	0.1	0.6	**21.8**	**22.5**
γ_{BR}	$0.1/10^3$	–	–	–	1.4
α^0_{CB}	$0.1/10^3$	–	–	**21.7**	**21.9**
δx^0_{BR}	100	–	–	0.4	**12.6**
δy^0_{BR}	100	–	–	0.4	**12.6**
δz^0_{BR}	100	–	–	–	0.8
δx^0_{CB}	100	–	–	0.4	**12.6**
γ^0_{YX}	$0.1/10^3$	–	–	–	1.1
α^0_{ZY}	$0.1/10^3$	–	–	–	0.3
β^0_{ZX}	$0.1/10^3$	–	–	–	0.3
Workpiece setup errors					
e_x	100	0.4	**12.6**	0.2	**5.7**
e_y	100	0.4	**12.6**	0.2	**5.5**
e_a	$0.1/10^3$	**14.2**	**13.7**	**14.2**	**13.7**
e_b	$0.1/10^3$	**14.2**	**13.7**	**14.2**	**13.7**

influence of workpiece position errors, $(e_x, e_y) = (0.2, -0.2)$ mm, is eliminated. The difference from measured profiles in Setup (1) (Fig. 7b) is significantly reduced; the mean of the difference is reduced to -1.7 μm (the difference's standard deviation is 2.2 μm).

This machine's rotary axis location errors, shown in Table 1, were identified by using the static R-Test [30]. The identified values were: $\delta x^0_{BR} = 6.3$ μm, $\delta y^0_{BR} = 2.8$ μm, $\delta z^0_{BR} = 10.7$ μm, $\delta x^0_{CB} = 2.4$ μm, $\alpha^0_{CR} = 20.0$ μrad, and $\beta^0_{CR} = 19.6$ μrad. According to the sensitivity analysis presented in Table 3, their influence on the measured profiles are negligibly small, compared to the influence of workpiece setup errors.

Remark: To separately identify each machine geometric error shown in Table 1 from the measured profiles, its influence on measured profiles must be distinguishable to each other. This can be numerically checked by the condition number of the sensitivity matrix representing the relationship presented in Table 3. It would totally depend on the workpiece geometry to be measured. This analysis will be left for future study.

5. Conclusion

In three-axis on-machine measurement of a workpiece geometry using linear axes only, position and orientation errors in the workpiece setup are not a critical issue. They simply translate or tilt the measured profile. Similarly, in three-axis measurement,

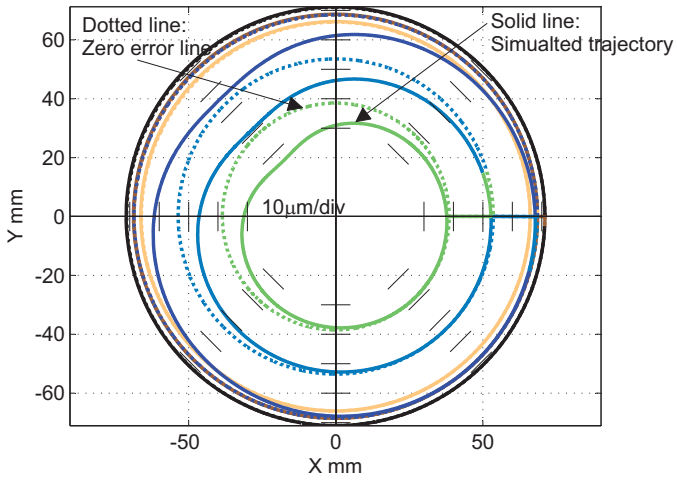

a)

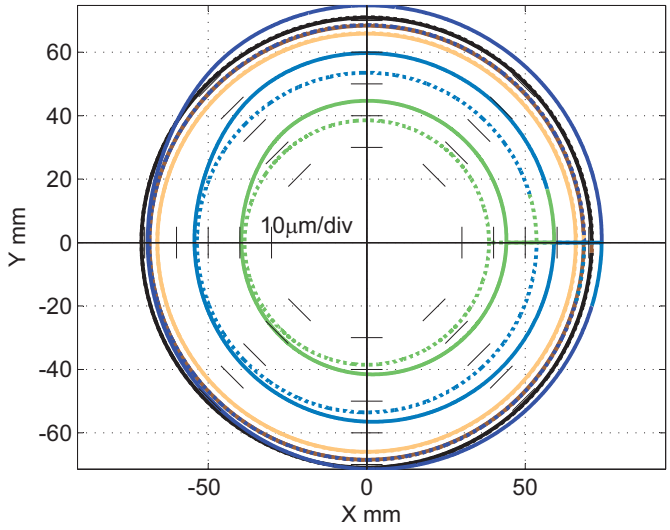

b)

Figure 11. Simulated surface profiles for Setup (2), where the workpiece is placed away from C-axis centerline. a) Influence of C-axis position error in X, $\delta x^0_{BR} = 100$ μm. b) Influence of workpiece position error in X, $e_x = 100$ μm. The simulated profile error is magnified 1,000 times and plotted in the radial direction.

linear axis error motions are directly copied as the geometric error of the measured profile. In five-axis measurement with rotating the workpiece, the influence of workpiece setup errors and rotary axis geometric errors must be formulated by using the five-axis kinematic model.

As a practical application example, this paper studied the error contributors in the scanning measurement of an axis-symmetric part. This paper presents the sensitivity analysis to assess the contribution of 1) position and orientation errors of linear and rotary axis average lines, and 2) position and orientation errors of workpiece. An experiment showed a significant difference in the measured geometry (1) when the

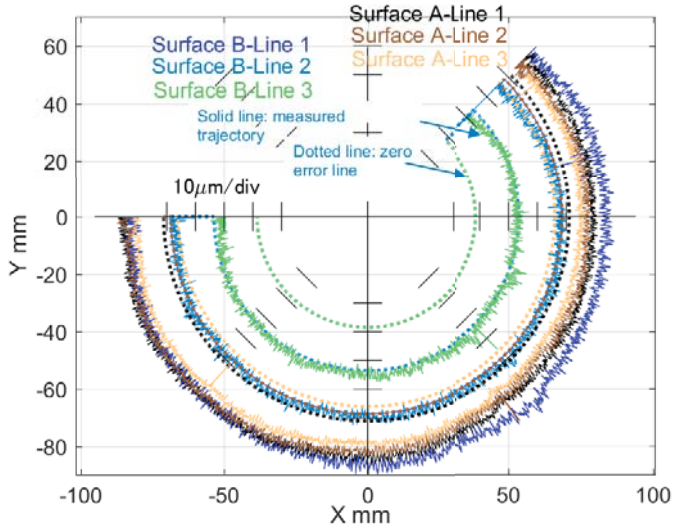

Figure 12. Difference in the profiles measured in Setup (2) (Fig. 8b) from those measured in Setup (1) (Fig. 7b). The difference is magnified 1,000 times and plotted in a radial direction from the corresponding "zero error line."

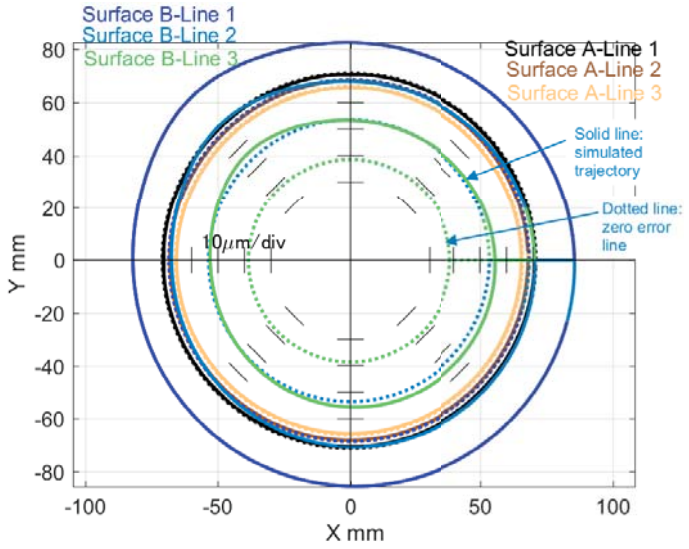

Figure 13. The simulated influence of the workpiece position error, $(e_x, e_y) = (0.2, -0.2)$ mm, on the profiles in Setup (2).

workpiece is placed concentric to the axis of rotation, and 2) when it is placed away from the axis of rotation. The present sensitivity analysis clarified that this difference was likely caused by the position error in the workpiece setup. As a potential application of the present kinematic model, the compensation of its influence on measured profiles is presented.

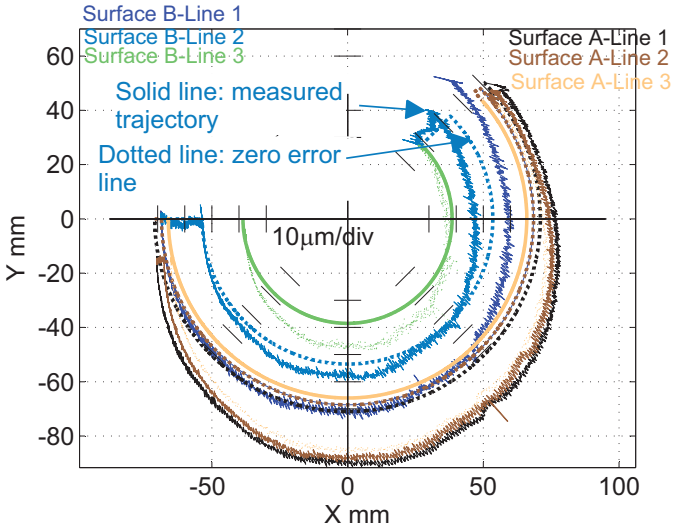

Figure 14. Measured profiles for Setup (2), where the influence of workpiece position errors, $(e_x, e_y) = (0.2, -0.2)$ mm, is eliminated.

References

[1] Savio E, De Chiffre L, Schmitt R (2007) Metrology of freeform shaped parts, CIRP Annals – Manufacturing Technology, 56(2): 810-835.

[2] Schwenke H, Neuschaefer-Rube U, Pfeifer T, Kunzmann (2002) Optical Methods for Dimensional Metrology in Production Engineering, CIRP Annals – Manufacturing Technology, 51(2): 685-699.

[3] Shacham D (2008) New Laser Technology in Turbine Blade Measurements. ASME 2008 9th Biennial Conf. on Engineering Systems Design and Analysis, 575-578.

[4] Nishikawa S, Ohno K, Mori M, Fujishima M (2014) Non-Contact Type On-Machine Measurement System for Turbine Blade, New Production Technologies in Aerospace Industry – 5th Machining Innovations Conference, Procedia CIRP 24: 1-6.

[5] Nisch S, Schmitt R (2010) Production integrated 3D measurements on large machine tools, Proc. of the Large Volume Metrology Conference, Chester, UK: 969

[6] Schmitt R, Peterek M, Morse E, Knapp W, Galetto M, Härtig F, Goch G, Hughes B, Forbes A, Estler W (2016) Advances in Large-Scale Metrology – Review and future trends, CIRP Annals – Manufacturing Technology, 65(2): 643-665.

[7] Mears, L., Roth, J. T., Djurdjanovic, D., Yang, X., Kurfess, T. (2009) Quality and Inspection of Machining Operations: CMM Integration to the Machine Tool, Journal of Manufacturing Science and Engineering, 131(5): 051006.

[8] Mutilba U, Gomez-Acedo E, Kortaberria G, Olarra A, Yagüe-Fabra JA (2017) Traceability on Machine Tool Metrology: A Review, Sensors, 17(7): 1605

[9] Takaya Y (2014) In-Process and On-Machine Measurement of Machining Accuracy for Process and Product Quality Management: A Review, International Journal of Automation Technology, 8(1): 4-19.

[10] Schmitt R, Peterek M (2015) Traceable measurements on machine tools – Thermal influences on machine tool structure and measurement Uncertainty. Procedia CIRP, 33: 576-580.

[11] Acko B, Klobucar R, Acko M (2015) Traceability of In-process Measurement of Workpiece Geometry, Procedia Engineering, 100: 376-383.

[12] Viprey F, H. Nouira, S. Lavernhe, C. Tournier (2016) Novel multi-feature bar design for machine

tools geometric errors identification, Precision Engineering, 46: 323-338.
[13] ISO 15530-3:2011, Geometrical product specifications (GPS) – Coordinate measuring machines (CMM): Technique for determining the uncertainty of measurement – Part 3: Use of calibrated workpieces or measurement standards.
[14] ISO/TS 15530-4:2008, Geometrical Product Specifications (GPS) – Coordinate measuring machines (CMM): Technique for determining the uncertainty of measurement – Part 4: Evaluating task-specific measurement uncertainty using simulation.
[15] Hocken RJ, Simpson JA, Borchardt B, Lazar J, Reeve C, Stein P (1977) Three dimensional metrology, CIRP Annals - Manufacturing Technology, 26(1): 403-408.
[16] D. N. Reshetov, V. T. Portman: *Accuracy of Machine Tools*, ASME Press, New York, NY, USA, 1988.
[17] Abbaszaheh-Mir Y, Mayer JRR, Clotier G, Fortin C (2002) Theory and simulation for the identification of the link geometric errors for a five-axis machine tool using a telescoping magnetic ball-bar, International Journal of Production Research, 40(18): 4781–4797.
[18] Inasaki I, Kishinami K, Sakamoto S, Sugimura N, Takeuchi Y, Tanaka F (1997) Shaper generation theory of machine tools – its basis and applications, Yokendo, Tokyo (in Japanese).
[19] Ibaraki S, Kimura Y, Nagai Y, Nishikawa S (2015) Formulation of Influence of Machine Geometric Errors on Five-Axis On-Machine Scanning Measurement by Using a Laser Displacement Sensor, Journal of Manufacturing Science and Engineering, 137: 021013-1/11.
[20] Ibaraki S, Nagai Y (2017) Formulation of the influence of rotary axis geometric errors on five-axis on-machine optical scanning measurement – application to geometric error calibration by "chase-the-ball" test, International Journal of Advanced Manufacturing Technology, 92: 4263-4273.
[21] ISO 230-7:2006, Test code for machine tools – Part 7: Geometric accuracy of axes of rotation.
[22] ISO 230-1:2012, Test code for machine tools – Part 1: Geometric accuracy of machines operating under no-load or quasi-static conditions.
[23] Ibaraki S, Oyama C, Otsubo H (2011) Construction of an error map of rotary axes on a five-axis machining center by static R-test, International Journal of Machine Tools and Manufacture, 51(3): 190-200.
[24] Ibaraki S, Blaser P, Shimoike M, Takayama N, Nakaminami M, Ido Y (2016) Measurement of thermal influence on a two-dimensional motion trajectory using a tracking interferometer, CIRP Annals - Manufacturing Technology, 65(1): 483-486.
[25] ISO 1101:2017, Geometrical product specifications (GPS) – Geometrical tolerancing – Tolerances of form, orientation, location and run-out
[26] JCGM 100:2008, Evaluation of measurement data – Guide to the expression of uncertainty in measurement (GUM), 2008.
[27] Gebhardt M, Mayr J, Furrer N, Widmer T, Weikert S, Knapp W (2014) High precision grey-box model for compensation of thermal errors on 5-axis machine tools, CIRP Annals – Manufacturing Technology, 63(1): 509-512.
[28] Hong C, Ibaraki S (2012) Observation of Thermal Influence on Error Motions of Rotary Axes on a Five-Axis Machine Tool by Static R-Test, International Journal of Automation Technology, 6(2): 196-204.
[29] Ibaraki S, Ota Y (2014) A machining test to calibrate rotary axis error motions of five-axis machine tools and its application to thermal deformation test, International Journal of Machine Tools and Manufacture, 86, 81-88.
[30] Ibaraki S, Nagai Y, Otsubo H, Sakai Y, Morimoto S, Miyazaki Y (2015) R-Test Analysis Software for Error Calibration of Five-Axis Machine Tools –Application to a Five-Axis Machine Tool with Two Rotary Axes on the Tool Side–, International Journal of Automation Technology, 9(4): 387-395